Compressed image transmission in precoded OFDM VLC systems

Zhongpeng Wang (wzp1966@sohu.com)
Zhejiang University of Science and Technology https://orcid.org/0000-0002-8236-7054
Yingying Hou
Zhejiang University of Science and Technology
Zhizhuo Wang
Zhejiang University of Science and Technology

Research Article

Keywords: Visible light communication (VLC), orthogonal frequency division multiplexing (OFDM), image transmission, compressive sensing, precoding

Posted Date: February 15th, 2022

DOI: https://doi.org/10.21203/rs.3.rs-1053273/v1

Compressed image transmission in precoded OFDM VLC systems

Zhongpeng Wang , Yingying Hou, Zhizhuo Wang

[1] School of Information and Electronic Engineering, Zhejiang University of Science and Technology, Hangzhou 310023, China
Corresponding author: Zhongpeng Wang (e-mail: wzp1966@ sohu.com）.

Abstract. In this paper, a compressed image transmission scheme is proposed in a precoded orthogonal frequency division multiplexing (OFDM)-based visible light communication (VLC) system. First, an image is divided into sub-block images; then, each block image is sampled by block-based compressive sensing (BCS) based on the Hadamard sparse basis matrix with a partial DCT measurement matrix. The resulting data are transformed into bit stream, which is transmitted in a DFT precoded OFDM-based VLC. We propose an integrated end-to-end OFDM-based VLC system platform, including BCS, quantization, VLC link, and OFDM transmission. The simulation results prove the effectiveness of the proposed simulation platform. The bit error rate (BER) and peak signal-to-noise ratio (PSNR) performances of the simulation platform are evaluated as well. The simulation results show that different images result in different BER and PSNR performances in the proposed precoded OFDM-VLC system. The larger the information entropy of images, the better the PSNR and BER performances. In addition, the PAPR of the DFT precoded OFDM can be significantly reduced compared to that of the conventional OFDM for compressed image data.

Keywords: Visible light communication (VLC), orthogonal frequency division multiplexing (OFDM), image transmission,compressive sensing,precoding.

1 Introduction

With the rapid development of wireless communication networks, digital image transmission over wireless links has been widely researched. Low latency and high-speed data transmission are the main requirements of future wireless communication system designs. Compressive sensing (CS) can reconstruct a sparse signal from few measurements. The CS technique has been widely applied in image processing, wireless sensor network, wireless communications, etc. [1–3]. The application of CS can reduce the transmitted image data volume and power consumption of electronic devices. Recently, compressed image transmission has attracted increasing attention [4–6]. In [7], an efficient compressed image transmission scheme was proposed for wireless multimedia sensors networks based on orthogonal frequency division multiplexing (OFDM). To reduce the complexity of image CS, block compressive sensing (BCS) schemes are employed in an image CS framework [8, 9]. Howev-

er, these BCS schemes do not consider the transmission performance of the compressed image data in communication systems. In [10], a compressed image transmission scheme based on block CS was proposed for OFDM systems. In the proposed scheme, compression and encryption were achieved simultaneously. However, the precoding technique used to improve PAPR and BER performances was not considered in the proposed system.

On the other hand, visible light communication (VLC) has the advantages of being free of electromagnetic interference and having large spectrum resources; thus, it has been widely researched [11–13]. Integrating orthogonal frequency division multiplexing (OFDM) with VLC can improve the frequency efficiency of VLC systems. Unlike radio frequency (RF) OFDM, the baseband signal should be a real and positive valued signal before driving an LED. Direct current biased optical OFDM (DCO-OFDM) is commonly used in OFDM-VLC systems [14, 15]. Utilizing Hermitian symmetry and DC bias, the DCO-OFDM baseband signal is real and positive valued. Our research mainly examines the transmission performance of compressed images in DCO-OFDM systems over visible light links. The investigated results can be widely applied to other types of communication systems.

In [16], Bayesian CS was employed to improve the channel capacity of an OFDM VLC system. However, to the best of our knowledge, methods to improve the performance of compressed image transmission in OFDM-based VLC has rarely been researched. In addition, similar to the RF-based OFDM, high peak-to-average power ratio (PAPR) is the main issue of OFDM-based VLC systems. Among all PAPR reduction methods, precoding is favored because it can reduce the PAPR without introducing signal distortion. Therefore, conventional precoding methods, such as discrete Fourier transform (DFT), discrete cosine transform (DCT), and Hadamard matrix, have been applied in optical OFDM [17–19].

Our research mainly focuses on studying and analyzing the BER and PSNR performances of the compressed image transmission in precoded OFDM-based VLC systems. The main contributions of this study are as follows.

First, we propose a BCS scheme using a Hadamard sparse basis with a chaotic DCT measurement matrix. Our research result shows that the smaller the information entropy of an image, the larger the PSNR value of the reconstructed image. Thereafter, we provide an integrated end-to-end OFDM-based VLC system platform, including block compressive sensing, quantization, VLC link, and OFDM.

Second, the BER and PSNR values of the compressed images are measured using the proposed OFDM-VLC transmission experiment platform. The simulation results show that different images yield different BER and PSNR performances in our proposed compressed image transmission system. The larger the information entropy of an image, the better the BER and PSNR of the transmission OFDM-VLC. This is contrary to the BCS scheme without transmission. In addition, the PSNR is barely improved at a high SNR region.

Third, to improve the PAPR performance of the proposed compressed image systems, DFT precoding is used. Among several precoding methods, the DFT precoding has the best PAPR reduction performance in the proposed compressed image transmission OFDM-VLC system.

Thus, our simulation experiment results prove the effectiveness of the compressed image transmission using the DFT precoded OFDM-based VLC systems. This study presents an integrated compressed image transmission over a VLC link with low PAPR and low computational complexity. The remainder of this paper is organized as follows. In section II the proposed scheme principles, which include block image compressive sensing, quantization, DFT precoding, OFDM modulation and demodulation, are introduced. In section III, the simulation and analysis are presented. Finally, conclusions are drawn in section IV.

2 System Principle

Here, we present an end-to-end compressed image transmission over wireless VLC systems. The transmitter side of the proposed system consists of compressed sampling, quantization, precoding, and OFDM modulation. In the following sections, each of processing step of the proposed system is described in detail.

2.1 Block Compressive Sensing Scheme

We first introduce the image-based BCS scheme, which is employed in reference [20]. The main idea is that the sampling and reconstruction of each block image are performed individually column by column. Compared to the entire image CS, BCS can minimize the computational complexity of CS. However, the block size affects the reconstructed image quality. Therefore, a good tradeoff between the complexity and reconstructed image PSNR can be obtained by optimizing the block size. Fig.1 shows the proposed image block CS scheme. The original image is first divided into many distinct blocks, sparsified by the Hadamard sparse basis matrix. Then, each of the resulting saprsified data is compressively sampled by a partial DCT measurement matrix. Finally, the obtained compressed data are quantized and transformed into a bitstream.

In our proposed BCS scheme, each block is CS sampled using the same measurement matrix. An $N \times N$ image is divided into many small blocks with size $B \times B$. The number of sub-blocks is $(N/B)\times(N/B)$. The jth image block is denoted as $\mathbf{x}_j$ with size $B \times B$. The qth column of $\mathbf{x}_j$, represented as $\mathbf{x}_j^q$, is compressively measured by a measurement matrix $\mathbf{\Phi}_B$ with length $M_B \times B$ ($M_B < B$), whose measured data are expressed as follows:

$$\mathbf{y}_j^q = \mathbf{\Phi}_B \mathbf{x}_j^q = \mathbf{\Phi}_B(\mathbf{\Psi}_B \mathbf{s}_j^q), \quad q = 1,\mathrm{L}\ ,B, \tag{1}$$

where $\mathbf{x}_j^q = \mathbf{\Psi}_B \mathbf{s}_j^q$. Further, $\mathbf{s}_j^q$ is the sparse coefficients, $\mathbf{\Phi}_B$ denotes a partial DCT measurement matrix with size $M_B \times B$ ($M_B < B$), and $\mathbf{\Psi}_B$ denotes a sparse Hadamard basis matrix with size $B \times B$. In the compressive sensing framework, the compressive ratio (CR) of CS is often defined as M_B / B.

After all columns $\mathbf{s}_j$ are measured, the obtained measured data $\mathbf{y}_j$ with size $M_B \times B$ is expressed as follows:

$$\mathbf{y}_j = \mathbf{\Phi}_B \mathbf{x}_j = \mathbf{\Phi}_B (\mathbf{\Psi}_B \mathbf{s}_j), \quad (2)$$

where $\mathbf{y}_j = \left[\mathbf{y}_j^1 \quad \text{L} \quad \mathbf{y}_j^B\right]$ and $\mathbf{s}_j = \left[\mathbf{s}_j^1 \quad \text{L} \quad \mathbf{s}_j^B\right]$. Each image block is measured using (1) or (2).

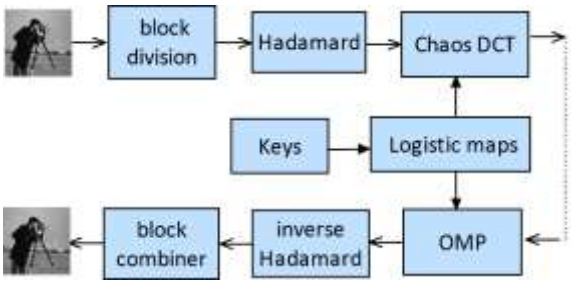

Fig. 1. Block diagram of the proposed block CS scheme

The DCT measurement matrix $\mathbf{\Phi}_B$ can be constructed using the following method [10]. First, we generated a chaotic sequence from a logistic map expressed as follows [21]:

$$x_{i+1} = \mu x_i (1 - x_i), \; q_i \in (0,1), \quad (3)$$

where $\mu \in [3.57, 4]$ is a control parameter. The resulting chaotic sequence $\mathbf{x} = \left[x_1 \quad x_2 \quad \text{L} \quad x_B\right]$ is processed according to the following formula to obtain an integer chaotic sequence.

$$q(n) = \text{mod}(\text{floor}((x_n + 100) \times 10^A), B) + 1 \quad (4)$$

where $q(n)$ denotes the element of the obtained integer chaotic sequence $\mathbf{q}$ with size of B. Where floor(x) returns the values of x to the nearest integers less than or equal to x, and mod(x, B) returns the remainder of x divided by B. A is related to the resolution of digital signal processing (DSP), which is set to be 10 in this work.[20] Then, the obtained integer chaotic sequence $\mathbf{q}$ can be used to scramble a conventional DCT matrix. Assume that a matrix is a conventional DCT matrix $\mathbf{\Phi}_{\mathbf{DCT}}$ with size $B \times B$. A chaotic integer sequence $\mathbf{q}$ with size $B \times 1$ is generated as a base logistic map. A traditional DCT matrix $\Phi_{DCT} = \left[F(1) \quad F(2) \quad \ldots \quad F(B)\right]^T$ is scrambled by the chaotic integer sequence $\mathbf{q} = \left[q(1) \quad q(2) \quad \ldots \quad q(B)\right]^T$. The obtained chaotic DCT matrix can be expressed as

$$\mathbf{\Phi}_{chaos} = \left[F(q(1)) \quad F(q(2)) \quad \text{L} \quad F(q(B))\right]^T, \quad (5)$$

where $F(i)$ denote the i-th row vector of a matrix with size $B \times B$. Finally, the former M_B rows are chosen to form the partial chaotic DCT measurement matrix, which is expressed as

$$\mathbf{\Phi}_B = \left[F(q(1)) \quad F(q(2)) \quad \text{L} \quad F(q(M_B))\right]^T. \quad (6)$$

In this study, the DCT measurement matrix described in (6) can be used in the reconstructed algorithm of CS. Based on the above measurement matrix, the sparse coefficients vector $\mathbf{s}_j^q$ can be solved using the following optimization problem:

$$\hat{\mathbf{s}}_j = \arg\min_{\mathbf{s}_j} \left\| \mathbf{s}_j^q \right\|_1 \text{ subject to } \mathbf{y}_j^q = \Phi_B \mathbf{x}_j^q, \tag{7}$$

where $\left\| \mathbf{s}_j^q \right\|_1$ denotes the $l_1 - norm$. Based on the reconstructed sparse signal $\hat{\mathbf{s}}_j$, the original signal $\mathbf{x}_j^q$ can be recovered via $\mathbf{x}_j^q = \Psi \mathbf{s}_j^q$. In this study, a conventional orthogonal matching pursuit (OMP) reconstructed algorithm [22] is used in the proposed BCS framework. The proposed BCS scheme is based on block image acquisition. Owing to the application of the proposed BCS scheme, the storage space for the measurement matrix can be reduced, and the reconstruction speed can be improved.

2.2 Quantization

For a digital communication system, the compressed data must be transformed into a bit steam. Therefore, a quantization operation is used on the resulting compressed data. In this study, a uniform quantizer is employed. The quantization operation is defined as follows [23]:

$$\mathbf{Y}_{i,j}^{\text{int}} = round(255 \times (\mathbf{Y}_{i,j} - \min) / (\max - \min)), \tag{8}$$

where "max" and "min" denote the maximum and minimum values of the measurement data matrix and $\mathbf{Y}_{i,j}$ states the i$^{\text{th}}$-row and j$^{\text{th}}$-column of the entire measured image data matrix. Then, the obtained integer number $\mathbf{Y}_{i,j}^{\text{int}}$ is transformed into a bit stream.

2.3 Proposed Compressed Image Transmission System

In this study, we mainly focus on analyzing the transmission performance of a compressed image in precoded OFDM-VLC systems. Fig. 2 depicts the proposed compressed image transmission OFDM-VLC system. According to the principle described in Fig. 1, the generated compressed image data are quantized using (8), and then the resulting data are transformed into a bit stream. Subsequently, the obtained bit stream is transformed into 16-QAM symbols. Every M 16-QAM symbols form a symbol vector, which is expressed as follows:

$$\mathbf{S} = \left[S(a(1)) \quad S(a(2)) \quad \text{L} \quad S(a(M)) \right], \tag{9}$$

To reduce the PAPR of OFDM signals, the symbol vector $\mathbf{S}$ is transformed into a new domain symbol vector $\mathbf{Y} = \mathbf{QS}$, where $\mathbf{Q}$ is a DFT precoding matrix with size $M \times M$, which is defined as

$$\mathbf{Q} = \begin{pmatrix} q_{0,0} & q_{0,1} & \text{L} & q_{1,N-1} \\ q_{1,0} & q_{1,1} & \text{L} & q_{1,N-1} \\ \text{M} & \text{M} & \text{M} & \text{M} \\ q_{N-1,0} & q_{N-1,1} & \text{L} & q_{N-1,N-1} \end{pmatrix}. \tag{10}$$

Every entry of matrix $\mathbf{Q}$ can be written as

$$q_{i,j} = \exp\left(\frac{2\pi ij}{M}\right), \tag{11}$$

where $i = 0,\ 1,\ \mathrm{K},\ M-1$, $j = 0,\ 1,\ \mathrm{K},\ M-1$, and $q_{i,j}$ means the i[th] row and j[th] column of the DFT precoding matrix.

To generate a real-valued OFDM signal, the input symbols of IFFT are constrained by the Hermitian symmetry (HS). An input signal vector $\mathbf{X}$ with size N is formed, which consists of the signal vector $\mathbf{Y}$, symmetric conjugate symbol vector of $\mathbf{Y}$, and pilot data symbols. The formed N subcarriers symbols of IFFT are expressed as

$$X = \left[X(0)\quad X(1)\quad X(2)\quad \mathrm{L}\quad X(N-1)\right]. \tag{12}$$

The signal vector $\mathbf{X}$ is constrained to have HS and given as

$$\begin{aligned} X(k) &= X^*(N-k), \qquad k = 1,2,\mathrm{L}\ ,(N/2-1) \\ X(0) &= X(N/2) = 0 \end{aligned}. \tag{13}$$

Then, these subcarrier symbols are fed into the IFFT module to generate a real-valued signal $\mathbf{x}$ with size N, which is expressed as

$$x(n) = \frac{1}{N}\sum_{k=0}^{N-1} X(k)\exp\left(\frac{j2\pi kn}{N}\right), \qquad 0 \le n \le N-1. \tag{14}$$

In practical OFDM systems, clipping is commonly employed to reduce the cost of ADCs and DAC devices [24]. The definition of the clipping ratio is given as

$$\mathrm{CR} = A^2 / P_{av}, \tag{15}$$

where A^2 represents the predefined peak power threshold and P_{av} denotes the average signal power. After clipping, the clipped signal can be denoted as

$$\bar{x}(n) = \begin{cases} x(n) & |x(n)| \le A \\ A\dfrac{x(n)}{|x(n)|} & |x(n)| > A \end{cases}. \tag{16}$$

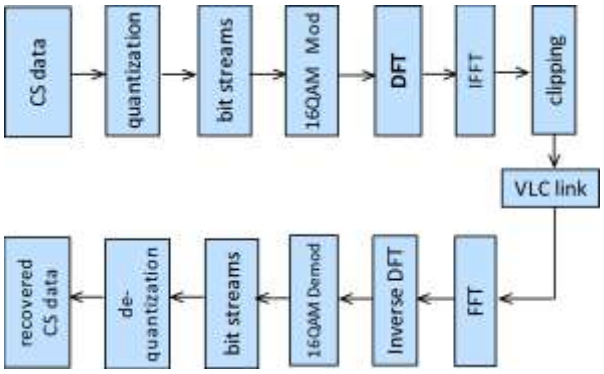

Fig. 2. Proposed compressed image transmission in the DFT precoded OFDM VLC system.

The resulting signal $\bar{\mathbf{x}}$ is transformed into an analog signal $\bar{\mathbf{x}}(t)$, which is added to DC bias. The DC-biasing level is related to the standard deviation of the signal $\bar{\mathbf{x}}$. Let β_{DC} be the DC bias level, which is given in [25] as

$$\beta_{DC} = \mu\sqrt{E\left|\bar{x}^2(t)\right|}\ , \tag{17}$$

where μ is a constant and β_{DC} is often defined as a bias with $10\log_{10}(\mu^2+1)$ dB. After $\bar{\mathbf{x}}(t)$ is added to a DC bias β_{DC}, the resulting signal is denoted as

$$\bar{\mathbf{x}}_{DCO}(t) = \begin{cases} 0, & \bar{x}(t) < -\beta_{DC} \\ \bar{x}(t) + \beta_{DC}, & \bar{x}(t) \geq -\beta_{DC} \end{cases}. \tag{18}$$

The generated signal $\bar{\mathbf{x}}_{DCO}(t)$ is fed to an LED, and the output optical signal of LED is propagated over the VLC link.

In this study, we consider an indoor VLC link wherein the LED is installed on the ceiling. Photodiode (PD) is positioned below the LED. Only the LOS path is considered because that the reflections are weak and negligible. It is assumed that a Lambertian emission pattern is employed in the LED. The path gain G of VLC link is given by [26, 27]

$$G = \begin{cases} \dfrac{1}{2\pi}(m+1)\cos^m(\phi)\dfrac{\mathrm{A}_{RX}}{d^2}\cos(\psi) & |\psi| \leq \psi_{FoV} \\ 0 & |\psi| \geq \psi_{FoV} \end{cases}, \tag{19}$$

where ϕ and d are the angle of irradiance and the LOS distance between the LED and PD, respectively; ψ and ψ_{FoV} are the angle of incidence and receiver field-of-view (FoV) semi-angle, respectively; and A_{RX} is the receiver collection area. A_{RX} is given by [27]

$$\mathrm{A}_{RX} = \frac{n^2}{\sin^2(\psi_{FoV})} A_{PD}\,, \tag{20}$$

where n denotes the refractive index of the optical concentrator and A_{PD} is the area of the PD. In (19), $m = \dfrac{-\log 2}{\log\cos\phi_{1/2}}$ denotes the Lambertian order, and $\phi_{1/2}$ is the semi-angle at half LED power. The receiver converts the optical signals to electrical signals via PDs. The resulting received electrical signals are given as

$$\begin{aligned} R_{PD}(t) &= \gamma G\bar{\mathbf{x}}_{DCO}(t) + N(t) \\ &= \gamma G(\beta_{DC} + \bar{x}(t)) + N(t) \\ &= \gamma G\bar{x}(t) + \gamma G\beta_{DC} + N(t) \end{aligned}\ , \tag{21}$$

where γ denotes the detector responsivity, $\bar{\mathbf{x}}_{DCO}(t)$ represents the received optical signal, $R_{PD}(t)$ represents the received signal, and $N(t)$ denotes the AWGN. After removing the DC bias, the received sample electrical signal can be expressed as

$$R(n) = \gamma G\bar{x}(n) + N(n)\,. \tag{22}$$

By performing an FFT operation on the two sides of (22), we can obtain the demodulated signal as

$$R(k) = \gamma G\bar{X}(k) + N(k)\,. \tag{23}$$

To simplify the above equation, we can rewrite it in the matrix form as follows:

$$\mathbf{R} = \gamma G\bar{\mathbf{X}} + \mathbf{N}\ . \tag{24}$$

After removing the symmetric conjugate symbol and pilot symbols from $\mathbf{R}$, we can obtain the signal $\hat{\mathbf{Y}}$ with size M, which is the estimation of $\mathbf{Y}$ and can be expressed as follows:

$$\hat{\mathbf{Y}} = \gamma G\hat{\mathbf{X}} + \hat{\mathbf{N}} \ . \tag{25}$$

Finally, performing an inverse precoding operation on $\hat{\mathbf{Y}}$, we obtain the estimation signal $\mathbf{S}$ of the original transmitted signal, which can be expressed as

$$\mathbf{P}^{-1}\hat{\mathbf{Y}} = \gamma G\mathbf{P}^{-1}\bar{\mathbf{X}} + \mathbf{P}^{-1}\hat{\mathbf{N}}, \tag{26}$$

$$\hat{\mathbf{S}} = \gamma G\mathbf{P}^{-1}\bar{\mathbf{X}} + \mathbf{P}^{-1}\hat{\mathbf{N}}. \tag{27}$$

Based on (27), the original transmitted modulated symbol vector $\hat{\mathbf{S}}$ can be obtained. Then, the modulation symbol vector is transformed into a bitstream, which is used to recover original image data.

3 Simulation Results And Analysis

We first evaluate the reconstructed performance of the proposed BCS scheme. Then, the performance of compressed image transmission in DFT precoded OFDM-VLC is evaluated in terms of BER and PSNR metrics in simulation. All the simulation experiments were conducted in MATLAB 2014b on a portable computer with a 2.20 GHz Intel Core i5 CPU and 4 GB memory, with Windows 7 operating system. A 16 QAM modulation format was employed regarding the simulation platform. Boats, Barbara, houses, parrots, and random images with 256×256 pixels are employed as test images. Tables 1 and 2 show the parameters of the VLC channel and OFDM system, respectively.

Table 1. Simulation parameters for VLC channels [27]

Room dimensions ($W\times L\times H$)	$5\times5\times3$ m^3
Light fixture height	3 m
Receiver height	0.85m
LED half luminous intensity semi angle $\phi_{1/2}$	60°
Modulation index α	10%
Receiver FoV ψ_{FoV}	60°
Lens refractive index n	1.5
PD responsivity γ	0.54 (A/W)
PD geometrical area A_{PD}	1 cm^2
Noise spectral density N_0	6.5×10^{-23} W/Hz

In the following experiments, we discover that the reconstructed image quality in CS and transmission performance of the compressed image in transmission systems are both related to the image entropy. The information entropy of images, which represents the randomness of the pixel values distribution, can be obtained as follows:

$$H(a) = \sum_{i=0}^{2^L-1} p(a_i) \log_2 \frac{1}{p(a_i)}, \qquad (28)$$

where $p(a_i)$ represents the probability of a_i and $L = 8$ for gray images. Theoretically, information entropy closer to 8 indicates a more random distribution of the pixel values. Table 3 shows the information entropy results for the plaintext images. Observe that the randomness of Barbara and parrots images are better than that of house and boat images. The last column in Table 3 is an image generated by random bits with an entropy value of 7.9894.

Table 2. Simulation system parameters

Modulation	16 QAM
Bit rate	100 Mbits/s
Sample rate	25 M samples /s
Modulation format	16 QAM
Number of subcarriers	256
Pilot subcarrier	8
Length of CP	32
Number Data subcarrier	192
Clipping ratio	12
Image block size	16×16
Logistic parameters	
Initial value x_0	$0.33\text{-}10^{-15}$
Control parameter μ	4

Table 3. Information entropy of different images

Image	house	boats	Barbara	parrots	random
Entropy	6.4930	7.1456	7.5252	7.4006	7.9894

3.1 PSNR Performance Of Block Compressive Sensing

In the CS framework, the PSNR is often used to evaluate the quality of reconstructed images and is defined as

$$PSNR = 10\log_{10}\left(255^2 / MSE\right), \qquad (29)$$

where the mean squared error (MSE) denotes the difference between the original and reconstructed images.

3.1.1 Effect of different measurement matrices on the PSNR of BCS

The performance of the proposed image BCS method, which is based on Hadamard sparse basis and DCT measurement matrices, is thoroughly examined. The measurement matrix plays a vital role in reconstructed PSNR performance. To evaluate the performance of our CS method, we compare the used measurement matrix with other exiting measurement matrices, namely, random matrix, Toeplitz matrix

[28], chaotic logistic matrix [29], partial chaotic Hadamard matrix [30], and partial DHT matrix [31]. The size of measurement matrix is $M \times 16$, where M denotes the row number of measurements and $M < 16$. The house image 256×256 is used as a test image.

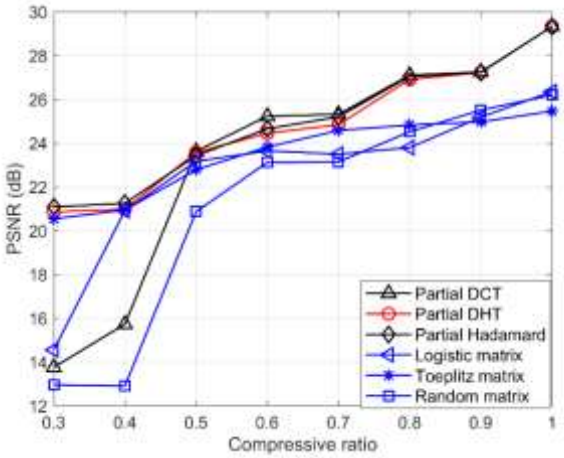

Fig. 3. PSNR Comparison with different measurement matrices

Fig. 3 demonstrates the comparison results regarding different measurement matrices to the Hadamard sparse basis matrix. Notice that the three measurement matrices, namely, partial DCT, partial DHT, and partial Hadamard matrices, can reconstruct the same image in the PSNR performance evaluations. In addition, the PSNR performances of these three measurement matrices are better than those of random, Toeplitz, and chaotic logistic matrices when the compressive ratio is higher than 0.5. However, the proposed BCS scheme worsens when the compressive ratio is smaller than 0.5.

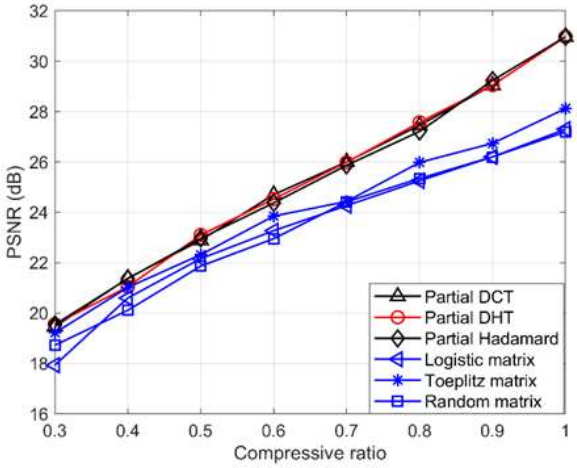

Fig. 4. PSNR comparison with different measurement matrices for CS using the whole image.

Regarding the entire image CS scheme, the PSNR comparison performance is demonstrated in Fig. 4. Similar results to those depicted in Fig. 3 can be obtained for the entire image CS. The only difference is the performances of the three structurally random measurement matrices, namely, partial DCT, partial DHT, and partial Hadamard matrices, are better than those of the random, Toeplitz, and chaotic logistic matrices for all compressive ratio case.

3.1.2 Effect of sub-block size on The PSNR and run timing of BCS without quantization

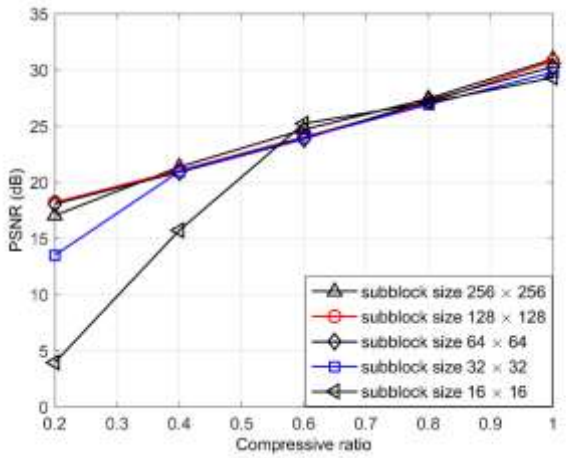

Fig. 5. Comparison of PSNR performances with different sub-block sizes.

Fig. 5 shows the comparison of PSNR performance of the proposed BCS scheme under different sub-block size. The test image is boats. Observe that the PSNR performances are almost identical when the compressive ratio value is lower than 0.6.

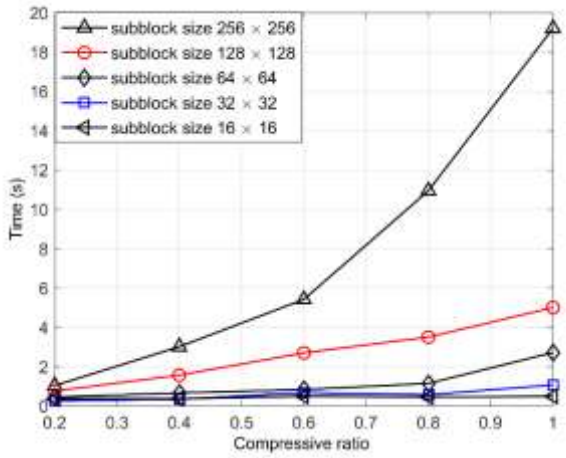

Fig. 6. Comparison of run time performances with different sub-block sizes.

Fig. 6 shows the relationship between the run times and compressive ratios for different sub-block size cases. The test image is again boats. Notice that the run times for a 16×16 sub-block size is the smallest. Therefore, considering the PSNR and run time performances, the optimum sub-block size is determined as 16×16.

Fig. 7 shows the comparison of PSNR performances of different test images without quantization. The sub-block size is 16×16. With an increasing compressive ratio, the PSNR performances of the reconstructed image are improved. The PSNR values of the reconstructed boats and house images are better than those of the reconstructed parrots and Barbara images.

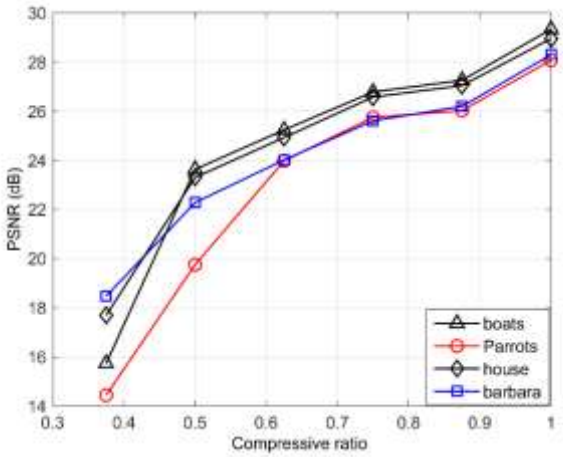

Fig. 7. PSNR performances with different images of 16×16 sub-blocks without quantization.

3.1.3 Comparison of the PSNR performance regarding different images with quantization

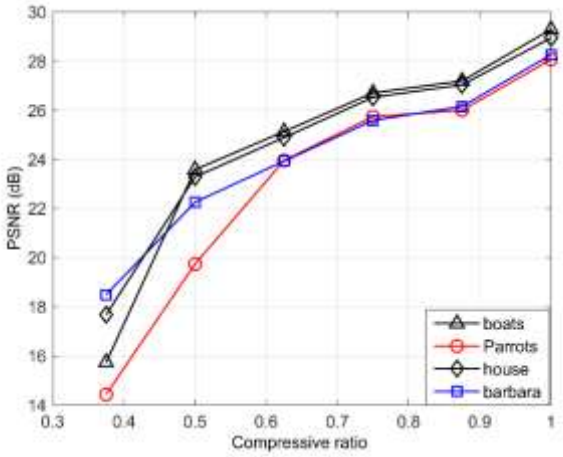

Fig. 8 PSNR performances with different images for a 16×16 sub-block size with quantization

Fig. 8 shows the comparison of PSNR performances of different test images for a 16×16 sub-block with quantization. Similar results to those depicted in Fig. 7 can be obtained here. The PSNR values of the reconstructed boats and house images are better than those of the reconstructed parrots and Barbara images. Moreover, the PSNR performance loss is minimal. Therefore, the effect of quantization error on PSNR performance is almost negligible. Based on the simulation results depicted in Figs. 7 and 8, different images yield different reconstruction performances in an image block compressive sensing framework. The larger the entropy of an image, the worse the reconstruction performance. Table 3 reports the entropy values of Barbara and parrots images, which are greater than those of house and boats images.

3.2 Transmission Performance

In this subsection, we evaluated the transmission performance of the compressed image in terms of PSNR and BER over the VLC channel. The simulation parameters used in this study are reported in Table 1. The former four test images with a size 256×256 reported in Table 3 are used. In the simulation experiments, each bock size is fixed at 16×16, and compressive ratio (CR) is fixed at 3/4. For the CS framework, CR is defined as M/N. Here, M and N denote the number of rows and columns of a measurement matrix, respectively. On the receiver side, a conventional OMP reconstructed algorithm is employed. Fig. 9 shows the relationship of BER and SNR of the proposed compressed image transmission in the DFT precoded OFDM-VLC system with different images. The experiment results show that different images yield different compression transmission performances. The BER performances of the compressed image transmission for Barbara and parrots images are better compared to the compressed image transmission for boats and house images. The larger the entropy value of an image, the better the BER performance of the compressed image transmission system.

In addition, we evaluated the BER performance of random bit streams over DFT precoded OFDM-VLC systems. Observe that the BER performances of the compressed image transmission for Barbara and parrots images are better compared to the OFDM-VLC system with a random bit source. The BER of the random bit source agrees well with the theoretical BER performance, which has a simple theoretical explanation: different images have different values of information entropy, leading to different compressed transmission performances of an OFDM-VLC system with different images.

In the following passage, we discuss the PSNR performance evaluation of the reconstructed images over the OFDM-VLC transmission system. In OFDM-VLC systems, two factors degrade the recovery quality of the reconstructed images. One is quantization, and the other is channel noise. Fig. 10 depicts a PSNR performance comparison with different image sources in OFDM-VLC systems under a compressive ratio of 3/4. Observe that the PSNR values are increasing with the increase in the SNR. However, when SNR is larger than 18 dB, the PSNR hardly increases. At low SNR, the PSNR performance is dominated by channel noise. Increasing the SNR can improve the transmission performance, which in turn improves the PSNR perfor-

mance. However, when SNR is larger than 18 dB, the PSNR performance of the reconstructed image hardly is improved with a further SNR increase. Similar to the results shown in Fig. 9, Fig. 10 shows that different images yield different PSNR performances in the proposed OFDM-VLC system. Evidently, the corresponding reconstructed PSNR performances of Barbara and parrots images are better than that of house and boat images. However, due to the poor CS performance of a random image generated from random bits, the PSNR performance of a compressed random image is the worst.

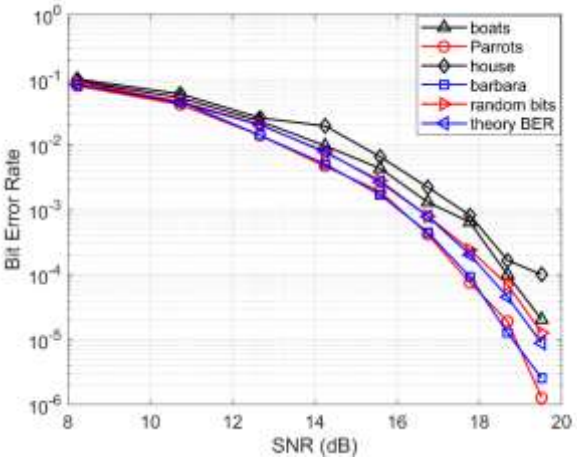

Fig. 9. BER performances of different image sources in DFT precoded OFDM-VLC systems with the compressive ratio of 3/4.

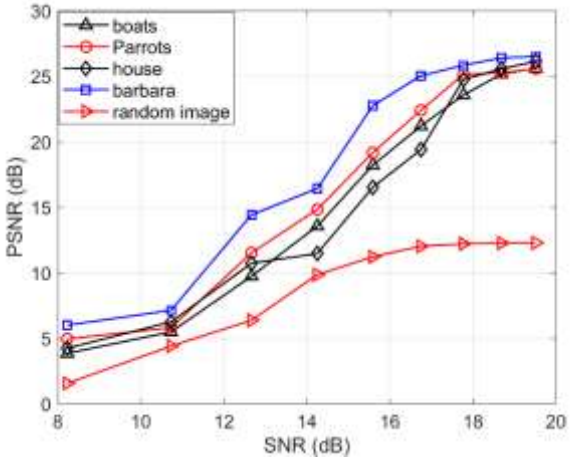

Fig. 10. PSNR performances of different image sources in DFT precoded OFDM-VLC systems with the compressive ratio of 3/4.

However, from Figs. 7 and 8, observe that the PSNR performances of the reconstructed Barbara and parrots images are worse than those of the reconstructed boats and house images. The experiment results shown in Figs. 9 and 10 contradict with the experimental results depicted in Figs. 7 and 8. Therefore, we infer that the random property of the compressed data impacts the PSNR performances of the reconstructed images.

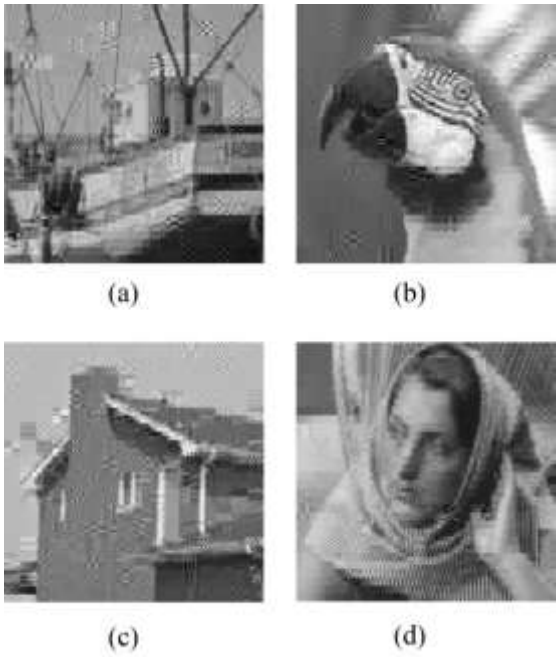

Fig. 11 Reconstructed images. (a) reconstructed boats image (PSNR=20.9679 dB , BER=0.0020), (b) reconstructed parrots image (PNSR=22.4531 dB, BER=2.5325e-04), (c) reconstructed house image (PSNR= 20.8369 dB, BER=0.0022), (d) reconstructed Barbara image (PSNR=23.7686 dB, BER=3.6919e-04).

Fig. 11 shows the reconstructed images in our proposed compressed image transmission in the DFT-precoded OFDM-VLC system under SNR = 17 dB and compressive ratio = 0.6. Figs. 11 (a), (b), (c), and (d) are the reconstructed boats, parrots, house, and Barbara images,respectively. The corresponding PSNR values of these reconstructed images are 20.9679, 22.4531, 20.8369, and 23.7686 dB, respectively. Moreover, the corresponding BER values of the reconstructed images are 2.3341e-04, 4.5767e-05, 5.8277e-04, and 7.1702e-05.

Fig. 12 shows the PSNR performance comparison of the received images in OFDM-VLC systems with SNR=17 dB cases. The PSNR values increase with an increase in the compressive ratio. However, when the CR value is greater than 0.6, the increase of the PSNR plateaus. Therefore, PSNR performances of different images have a different impact. In Fig. 12, random denotes an image generated from random

bits. The PSNR demonstrates poor performance due to the poor compressibility of the random images.

Based on these simulation results, different images yield different BER and PSNR performances in the proposed compressed image transmission OFDM-based VLC system. This differs from the OFDM-based random source.

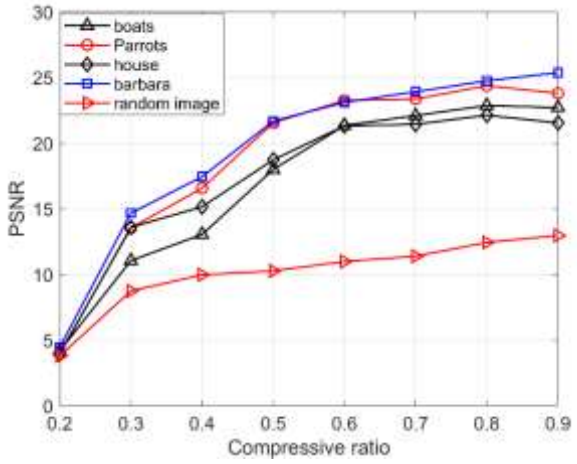

Fig. 12. PSNR performance comparison of the received images in an OFDM-VLC system under different compressive ratios.

3.3 PAPR Performance

High PAPR value is a disadvantage of the OFDM system. It can cause a great loss of power efficiency. Therefore, to mitigate this drawback, many reduction PAPR methods have been proposed. Among these methods, DFT precoding is a distortionless method and is widely employed in optical and RF OFDM systems. This study uses DFT precoding to minimize PAPR in the proposed compressed image transmission of OFDM-VLC systems. PAPR is described as the ratio of peak power and average power.

$$\text{PAPR} = \frac{\max\limits_{0\le n\le N-1}\left[\left|x(n)\right|^2\right]}{E\left\{\left|x(n)\right|^2\right\}}, \qquad (30)$$

where $E\{\cdot\}$ denotes the mathematical expectation operation. The complementary cumulative distribution function (CCDF) is often used to evaluate the PAPR performance of OFDM signals.

We measure the PAPR in the OFDM signal of the compressed image signal with different precoding matrices. In this figure, the test image is a house image. Fig. 13 shows the corresponding simulation results. The DFT precoding yields the best PAPR performance. For example, at CCDF=10^{-3}, the PAPR of DFT precoded 16-QAM OFDM of the compressed image can be reduced by approximately 8 dB compared to

that of the conventional 16-QAM OFDM for the compressed image. In addition, DFT has fast computational algorithms. Thus, we utilize DFT precoding to reduce the PAPR of OFDM signals. In addition, in practical OFDM systems, to reduce the dynamic range of input of a DAC, clipping is often employed. In this study, the clipping ratio is fixed at 12.

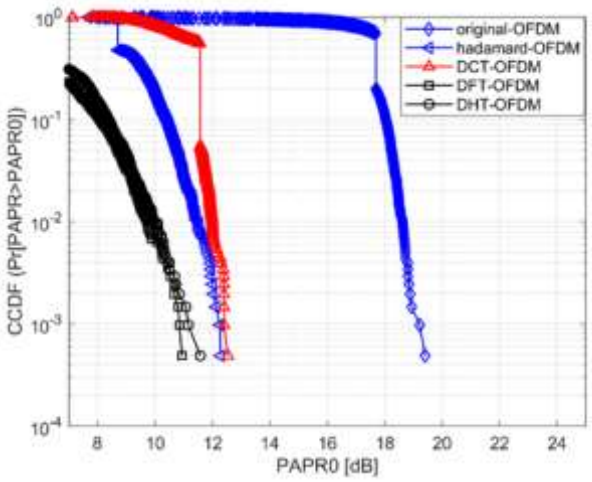

Fig. 13. Comparison of the PAPRs of the precoded 16-QAM OFDM signals for the com pressed image.

3.4 Performance Analysis

3.4.1 BER performance analysis

Based on these simulation results, we know that different images yield different BER transmission performances in a compressed image transmission system. The larger the information entropy of image, the better the BER of the proposed system. Furthermore, this leads to an improvement of the PSNR performance in the proposed transmission system. In our experiment, we calculated the average power of the transmitted signal with a varying compressed image source. According to the signal processing theory, the average of an OFDM signal with size of N can be calculated as follows:

$$P_{av} = \frac{1}{N}\sum_{n=1}^{N} x(n)\,. \tag{31}$$

The obtained OFDM signal powers using different compressed image sources are shown in Table 4

Table 4. Average power with different compressed images

sources	house	boats	Barbara	parrots	random bits
Power	0.9727	0.7517	0.6005	0.5708	0.7761

In this study, the 16-QAM modulation format is used. In fact, different 16-QAM symbol streams, which are generated from the different compressed image data, result

in different average power. This is because the random properties of different images are different. This leads to a non-equal probability distribution of constellation points in constellation space. Therefore, the generating non-equiprobable 16-QAM symbols processed in the proposed system simultaneously act as probabilistic shaping (PS) parameters [32, 33], which are widely studied in optical communication systems. The idea of PS is that the constellation points with equidistant space are assigned to different probabilities. To this end, the transmission performance reliability can be improved. Fig. 14 shows signal space diagram of 16-QAM, which is used in this study. From Fig. 14, notice that the four constellation points, s_5, s_7, s_{15}, and s_{13}, have the minimum symbol energy value. The average energy of signal can be reduced through arranging these constellation points with high probability.

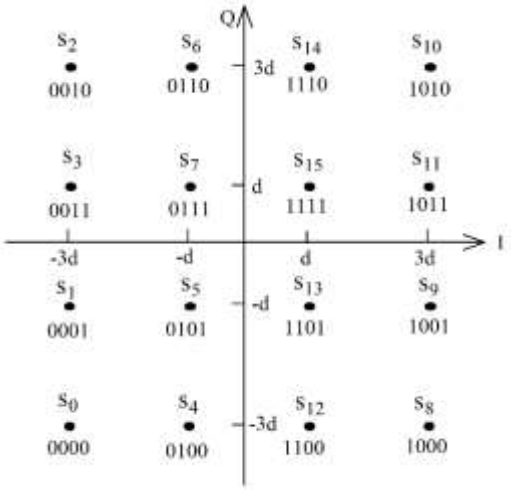

Fig. 14. Constellation points of the 16-QAM modulation format.

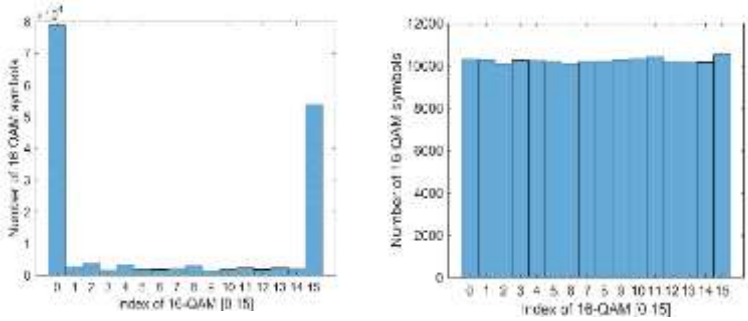

Fig. 15. Histogram analysis of 16-QAM: (a) with the compressed house image source and (b) with random bits source.

In following passage, we evaluate the constellation point distribution using histogram. Figs. 15 (a), and (b) are the measured constellation point results with compressed house image and random bits sources, respectively. From Fig. 15 (a), observe that the occurrence frequency of the high energy symbol s_0 (000) is the highest. In

contrast, the occurrence frequencies of each constellation symbol reported in Fig. 15 (b) are almost identical. Therefore, the average energy for the compressed house image is higher than that for random bits source. Furthermore, the average

power of the OFDM signal for the compressed house image is higher than that for random bits sources, which is confirmed in Table 4.

In Table 4, the average power of the OFDM signal for compressed house image data and random bits are reported as 0.9727 and 0.7762, respectively. Subsequently, we may compare the BER performances of these cases. The OFDM signal with random bits needs multiplexing a constellation scaling η to reach the same average power of OFDM signal with the compressed house image. The operation can be expressed as follows:

$$P_{house} = \eta^2 P_{random} , \tag{32}$$

where P_{house}, and P_{random} denote the average powers for the compressed house image and random bits sources, respectively.

Therefore, based on the experimental results reported in Table 4, with the same SNR value, the BER performance order for the sources reported in also in the table from poor to good is house, boat, random bits, Barbara, and parrots. This is agrees with the experiment results reported in Fig. 9.

3.4.2 Effect of entropy on the reconstructed performance of BCS

From the previously reported simulation results in Figs. 7 and 8, the reconstruction performance of BCS is deduced to be relative to the entropy values of an image. The larger the entropy of an image, the better the random property of the image. The compressibility of such an image is poor. On the other hand, the smaller the entropy of an image, the stronger the correlation between different pixels in an image. The compressibility of an image with high entropy value is better. Correspondingly, the reconstructed performance of BCS is better.

4 Conclusions

In this paper, we proposed a novel image block compressed image transmission scheme in DFT precoded OFDM-based VLC systems. In the compressive sensing phase, sub-block image was compressively sampled using Hadamard sparse basis and partial DCT measurement matrices. In the transmission phase, the conventional DFT precoding was implemented to reduce the PAPR performance of the OFDM signal. In the integrated simulation experiment platform, the BER and PSNR of different images were evaluated. The simulation results showed that different images yield different BER and PSNR performances with respect to the information entropy of image. The larger the image entropy, the better the BER and PSNR performances of the compressed data. In future studies, to improve the transmission performance of compressed data, we will further analyze how to optimize statistical features of the compressed image data.

Acknowledgments

This work was supported by the Key Laboratory of Universal Wireless Communications (BUPT), Ministry of Education, China (under KFKT-2020103); and Zhejiang Provincial Key Natural Science Foundation of China LZ21F010001.

Conflict of interest

The authors declared that they have on conflicts of interest to this work.

References

1. S. Ji, Y. Xue, and L. Carin, "Bayesian compressive sensing," *IEEE Trans. Signal Process*., vol. 56, no. 6, pp. 2346-2356, June 2008.
2. P. Zhang, L. Wang, X. Fang, H. He, H. Han, and B. Chen, "Secure transmission of compressed sampling data using edge clouds," *IEEE Trans. Industr. Inform.*, vol. 16, no. 10, pp. 6641-6651, Oct. 2020.
3. S. A. Nandhini, S. Radha, and P. Nirmala, "Compressive sensing for images using a variant of Toeplitz matrix for wireless sensor networks," *J. Real time Image Process.*, vol. 16, no.5, pp. 1525-1540, 2019.
4. L. Li, L. Liu, H. Peng, Y. Yang, and S. Cheng, "Flexible and secure data transmission system based on semitensor compressive sensing in wireless body area networks," *IEEE Internet Things J.*, vol. 6, no. 2, pp. 3212-3227, April 2019.
5. Z. Chen, X. Hou, X. Qian, and C. Gong, "Efficient and robust image coding and transmission based on scrambled block compressive sensing," *IEEE Trans. Multimedia*, vol. 20, no. 7, pp. 1610-1621, July 2018, doi: 10.1109/TMM.2017.2774004.
6. A. Pramanik and S. P. Maity, "On CS image reconstruction using LDPC code over radio mobile channel," *Wireless Pers Commun*., vol. 100, pp. 401-427, 2018.
7. A. Bouchemel, D. Abed and A. Moussaoui, "Enhancement of Compressed Image Transmission in WMSNs Using Modified u-Nonlinear Transformation," IEEE Communications Letters, vol. 22, no. 5, pp. 934-937, May 2018.
8. L. Zhu, H. Song, X. Zhang, et al., "A robust meaningful image encryption scheme based on block compressive sensing and SVD embedding," *Signal Processing*, no. 175, pp. 107629, 2020.
9. C. Pan, G. Ye, X. L. Huang, and J. Zhou, "Novel meaningful image encryption based on block compressive sensing," *Security Commun. Net.*, Volume 2019 , 2019, Art. ID 6572105.
10. Z. Wang, "Secure image transmission in wireless OFDM systems using secure block compression-encryption and symbol scrambling," *IEEE Access*, vol. 7, pp. 126985-126997, 2019, doi: 10.1109/ACCESS.2019.2939266.
11. S. Wu, H. Wang, and C. H. Youn, "Visible light communications for 5G wireless networking systems: from fixed to mobile communications," *IEEE Network*s, vol. 28, no. 6, pp. 41-45, 2014.
12. D. W. Dawoud, F. Héliot, M. A. Imran, and R. Tafazolli, "A novel unipolar transmission scheme for visible light communication," *IEEE Trans. Comm.*, vol. 68, no. 4, pp. 2426-2437, April 2020.

13. T. Q. Wang and X. Huang, "Fractional reverse polarity optical OFDM for high speed dimmable visible light communications," *IEEE Trans. Comm.*, vol. 66, no. 4, pp. 1565-1578, April 2018.
14. J. Armstrong and B. Schmidt, "Comparison of asymmetrically clipped optical OFDM and DC-biased optical OFDM in AWGN," *IEEE Comm. Lett.*, vol. 12, no. 5, pp. 343-345, May 2008.
15. T. Jiang *et al*., "Investigation of DC-biased optical OFDM with precoding matrix for visible light communications: Theory, simulations, and experiments," *IEEE Photonics Journal*, vol. 10, no. 5, pp. 1-16, Oct. 2018, Art no. 7906916.
16. Y.-Y. Won, D.-S. Seo, and S. M. Yoon, "White light-emitting diode based wireless orthogonal frequency division multiplexing link with improved transmission capacity using Bayesian compressive sensing," *Opt. Eng.* vol. 55, no. 4, 046101, 2016.
17. W. Zhongpeng, X. Jiangnan, L. Fan, and C. Lin, "Hadamard precoding for PAPR reduction in optical direct detection OFDM systems," *Optoelectronics Letters*, vol. 7, no. 5, pp. 0363-0366, Sep. 2011.
18. Y. Li, Y. Deng, J. He, S. He, and L. Chen, "DFT-spread combined with clipping method to reduce the PAPR in VLC-OFDM system," *Optoelectronics Letters*, vol. 13, no. 3, pp. 229-232, 2017.
19. A. A. E. Hajomer, X. Yang, and W. Hu, "Chaotic Walsh–Hadamard transform for physical layer security in OFDM-PON," *IEEE Photonics Technol. Lett.*, vol. 29, no. 6, pp. 527-530, 2017.
20. H. Guiqiang, X. Di, W. Yong, and X. Tao, "An image coding scheme using parallel compressive sensing for simultaneous compression-encryption applications," *Journal of Visual Communication & Image Representation*, Vol.44, pp. 116-127, 2017.
21. B. Stoyanov, K. Kordov, "Novel image encryption scheme based on Chebyshev polynomial and Duffing map," *Sci. World J.,* pp. 283639-283639, 2014.
22. J. A. Tropp and A. C. Gilbert, "Signal recovery from random measurements via orthogonal matching pursuit," *IEEE Trans. Info. Theory*, vol. 53, no. 12, pp. 4655-4666, 2007.
23. L. Gong, K. Qiu, C. Deng, and N. Zhou, "An image compression and encryption algorithm based on chaotic system and compressive sensing," *Opt. and Laser Technol.,* vol. 115, pp. 257-267, 2019.
24. D. J. G. Mestdagh, P. Spruyt, and B. Biran, "Analysis of clipping effect in DMT-based ADSL systems," *Proceedings of ICC/SUPERCOMM'94 - 1994 International Conference on Communications*, 1994, pp. 293-300 vol. 1.
25. S. D. Dissanayake and J. Armstrong, "Comparison of ACO-OFDM, DCO-OFDM and ADO-OFDM in IM/DD Systems," *J. Light. Technol.*, vol. 31, no. 7, pp. 1063-1072, April 1, 2013.
26. B. C. Jeffrey and M. K. Joseph, "Model of non-directed wireless infrared channels," *IEEE Trans. Commun,* vol. 45, pp. 1260-1268, 1997.
27. A. Mostafa and L. Lampe, "Physical-layer security for MISO visible light communication channels," *IEEE J. Sel. Areas Commun.*, vol. 33, no. 9, pp. 1806-1818, Sept. 2015, doi: 10.1109/JSAC.2015.2432513.
28. J. Haupt, W. U. Bajwa, G. Raz, and R. Nowak, "Toeplitz compressed sensing matrices with applications to sparse channel estimation," *IEEE Trans. Info. Theory*, vol. 56, no. 11, pp. 5862-5875, Nov. 2010.
29. L. Gong, K. Qiu, C. Deng, and N. Zhou, "An image compression and encryption algorithm based on chaotic system and compressive sensing," *Optics & Laser Technology*, vol. 115, pp.257-267, 2019.

30. N. Zhou, A. Zhang, J. Wu, D. Pei, Y. Yang, “Novel hybrid image compressive-encryption algorithm based on compressive sensing,” Optik, vol. 125, no. 18, pp. 5075-5080, 2014.
31. Z. Wang, L. Liu, S. Chen, et al., “Secure image block compressive sensing using chaotic DCT sparse basis and partial chaotic DHT measurement matrix,” Sensing and Imaging, vol. 21, no. 22, 2020.
32. Y. Yao, K. Xiao, B. Xia, and Q. Gu, "Design and analysis of rotated-QAM based probabilistic shaping scheme for Rayleigh fading channels," IEEE Trans. Wirel. Commun., vol. 19, no. 5, pp. 3047-3063, May 2020, doi: 10.1109/TWC.2020.2970007.
33. D. Pilori, L. Bertignono, A. Nespola, F. Forghieri, and G. Bosco, "Comparison of probabilistically shaped 64QAM with lower cardinality uniform constellations in long-haul optical systems," J. Light. Technol., vol. 36, no. 2, pp. 501-509, Jan. 2018, doi: 10.1109/JLT.2017.2752842.